A Quad-Polarization Reconfigurable Antenna With Suppressed Cross Polarization Based on Characteristic Mode Theory

Long Zhang, *Member, IEEE*, Yuhang Sun, Yejun He, *Senior Member, IEEE*, Sai-Wai Wong, *Senior Member, IEEE*, Chunxu Mao, *Member, IEEE*, Lei Ge, *Senior Member, IEEE*, and Steven Gao, *Fellow, IEEE*

***Abstract*— Based on characteristic mode theory (CMT), a quad-polarization reconfigurable antenna with suppressed cross polarization is proposed in this article. The proposed antenna is composed of the radiator, excitation units, and feeding network. A square conductive slab (SCS) is used as the main radiator, which is designed elaborately by characteristic mode analysis (CMA). Different modes of the radiator are stimulated selectively by four groups of balanced inductive exciters (BIEs) to realize horizontal polarization (HP), vertical polarization (VP), left-hand circular polarization (LHCP), and right-hand circular polarization (RHCP). Two p-i-n diodes are embedded into the feeding network to switch the excitation states of the four groups of BIEs, thereby achieving quad-polarization reconfiguration. More importantly, a novel method exploiting the CMA is adopted for achieving low cross polarization. By means of introducing the orthogonal mode, the cross-polarization component of the fundamental mode can be canceled out by the co-polarization component of the orthogonal mode, which greatly reduces the cross polarization from −10 to −40 dB in the two principal planes. The measurement results demonstrate that the quad-polarization agility and a cross-polarization level around −30 dB under all polarization states are achieved simultaneously, verifying the functionality and reliability of the proposed method.**

***Index Terms*— Characteristic mode theory (CMT), low cross polarization, polarization reconfigurable antenna.**

I. Introduction

IN PAST decades, polarization reconfigurable antennas have attracted considerable interests for their advantages in increasing the communication system capacity [1] and realizing multiple orthogonal channels for frequency reuse [2].

Typically, there are two ways to implement polarization reconfigurable antennas. The first one is by using reconfigurable radiators, such as the reconfigurable square patch antennas [3], [4], the reconfigurable circular patch antennas [5], [6], the reconfigurable planar dipole antennas [7], [8], and the reconfigurable monopole antennas [9]. Due to the RF switches embedded in the radiator, the surface current on the antenna can be easily changed, thereby achieving polarization reconfiguration. Nonetheless, the introduction of RF switches in the radiator and the interference of the bias circuit nearby the radiator will affect the antenna performance [10]. The other method widely utilized in designing polarization reconfigurable antennas is to employ a reconfigurable feeding network. By switching different feeding paths, different feeding phases or positions can be configured, which helps achieve polarization reconfiguration. A polarization reconfigurable patch antenna realized by mechanically changing the relative position between the feeding probe and patch antenna was proposed in [11], which was inconvenient to perform. By using electronically reconfigurable feeding networks, the tri-polarization reconfigurable antenna [12] and the quad-polarization reconfigurable antennas [13], [14] were implemented. Besides the two aforementioned methods, the polarization reconfigurable antennas can also be obtained by metasurface antennas [15], [16].

Recently, the characteristic mode theory (CMT) received a renewed and boosted interest in the field of antenna design for various applications [17], [18]. The CMT, based only on the geometry of antennas, provides an insightful view of the scattering and radiation properties of a radiating structure and offers a valuable guidance for antenna design [19]–[21]. By analyzing the characteristic currents and fields, various kinds of antennas with good performances were proposed, including the multiband antenna [22], pattern reconfigurable antenna [23], wideband antennas [24], [25], and MIMO antennas [26]–[29]. The CMT can also be used to design polarization reconfigurable antennas. In [30], a tri-polarization reconfigurable antenna was achieved by exciting different characteristic modes (CMs).

Although numerous polarization reconfigurable antennas were proposed, a few of them took into account the radia-

Manuscript received June 28, 2019; revised June 8, 2020; accepted June 28, 2020. Date of publication August 19, 2020; date of current version February 3, 2021. This work was supported in part by the National Natural Science Foundation of China under Grant 61801299, in part by the Natural Science Foundation of Guangdong Province under Grant 2020A1515011037, in part by the Mobility Program for Taiwan Young Scientists under Grant RW2019TW001, and in part by the Shenzhen Science and Technology Program under Grant GJHZ20180418190529516 and Grant JSGG20180507183215520. *(Corresponding author: Yejun He.)*

Long Zhang, Yuhang Sun, Yejun He, Sai-Wai Wong, and Lei Ge are with the College of Electronics and Information Engineering, Shenzhen University, Shenzhen 518060, China (e-mail: long.zhang@szu.edu.cn; heyejun@126.com).

Chunxu Mao is with the 5G Innovation Center (5GIC), Institute for Communication Systems (ICS), University of Surrey, Guildford GU2 7XH, U.K. (e-mail: c.mao@surrey.ac.uk).

Steven Gao is with the School of Engineering and Digital Arts, University of Kent, Canterbury CT2 7NT, U.K. (e-mail: s.gao@kent.ac.uk).

Color versions of one or more of the figures in this article are available online at https://ieeexplore.ieee.org.

Digital Object Identifier 10.1109/TAP.2020.3016384

tion performance, such as the cross-polarization level. Antennas with low cross polarization are essential for various applications, such as the base stations [31] and high-precision global navigation satellite system [32]. Therefore, it would be significant to design an antenna with polarization agility and low cross polarization simultaneously.

In this article, a quad-polarization reconfigurable antenna with suppressed cross polarization is presented by using the characteristic mode analysis (CMA). The proposed antenna consists of a square conductive slab (SCS) stimulated by four groups of balanced inductive exciters (BIEs) [33] and a reconfigurable feeding network controlled by two p-i-n diodes. The SCS acts as the main radiator, whereas the four BIEs are responsible for the excitation of the CMs. By controlling the ON/OFF states and phase differences of the four BIEs, different polarizations can be achieved, including the horizontal polarization (HP), vertical polarization (VP), left-hand circular polarization (LHCP), and right-hand circular polarization (RHCP). More importantly, by analyzing the amplitude and phase of the far-field characteristic electric field (CEF) of the SCS and skillfully selecting the feeding strategy, the cross-polarization component of the fundamental mode can be canceled out by the co-polarization component of the orthogonal mode, thereby achieving low cross polarization in the two principal planes. It is demonstrated by the measurement results that the cross polarization of the proposed antenna under all polarization states can be reduced to lower than −30 dB. The presented method is believed to be applicable for other kinds of antennas reducing the cross polarization.

This article is organized as follows. In Section II, the CMs of the proposed antenna are analyzed and discussed, and meanwhile, the corresponding full-wave simulation with ideal feeding ports is provided to verify the analysis. Based on these analyses, a novel method to suppress the cross polarization is proposed. Section III is devoted to illustrate how the quad-polarization reconfiguration is realized. The measurement results and relevant discussions are provided in Section IV. Finally, a conclusion is given in Section V.

II. Characteristic Modes Investigation

A. Brief Introduction of Characteristic Mode Theory

On the basis of the CMT, the total current distribution ($\boldsymbol{J}_{tot}$) on a complex object can be decomposed into the linear superposition of a series of orthogonal current modes ($\boldsymbol{J}_n$), which depends on the geometry and dimensions of the object. The total current distribution ($\boldsymbol{J}_{tot}$) is expressed as

$$\boldsymbol{J}_{tot} = \sum_n \alpha_n \boldsymbol{J}_n \tag{1}$$

where α_n represents a complex coefficient related to the current mode $\boldsymbol{J}_n$, generally known as modal weighting coefficient (MWC). The magnitude of α_n describes how a particular mode contributes to the total current density when the excitation is ON. The phase of α_n is the ultimately excited phase of the corresponding current mode $\boldsymbol{J}_n$. The MWC α_n can be calculated as

$$\alpha_n = \frac{V_n^i}{1 + j\lambda_n} = \frac{< \boldsymbol{J}_n, \boldsymbol{E}^i >}{1 + j\lambda_n}. \tag{2}$$

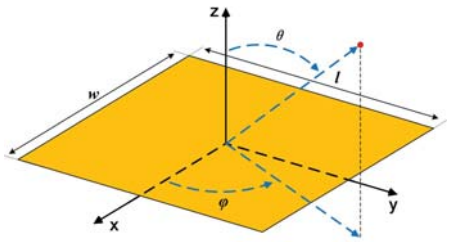

Fig. 1. SCS, $w = l = 65$ mm.

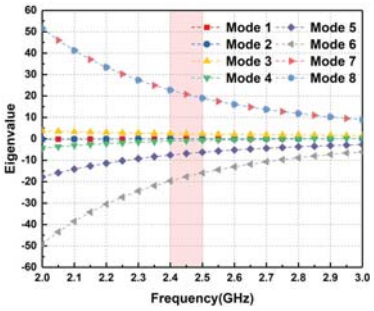

Fig. 2. Eigenvalues of the first eight modes.

The modal excitation coefficient V_n^i depends on the position, magnitude, phase, and polarization of the applied excitations, which can be further expressed as the inner product of the characteristic current ($\boldsymbol{J}_n$) and excited electric field ($\boldsymbol{E}^i$). The magnitude of eigenvalue λ_n indicates how well the nth mode can be excited. The smaller the magnitude of λ_n is, the more effectively the nth mode radiates. When λ_n is negative ($\lambda_n < 0$), the relevant mode is identified as a capacitive mode, whereas an inductive mode is recognized when λ_n is positive ($\lambda_n > 0$). In particular, the nth mode resonates when λ_n equals to zero ($\lambda_n = 0$).

Due to the linear dependence between the characteristic current mode and the CEF, the total radiated electric field ($\boldsymbol{E}_{tot}$) in the far field can be written as

$$\begin{aligned} \boldsymbol{E}_{tot} &= \sum_n \alpha_n \boldsymbol{E}_n \\ &= \sum_n \alpha_n \left(E_{\theta n}\, \boldsymbol{e}_\theta + E_{\varphi n}\, \boldsymbol{e}_\varphi\right) \end{aligned} \tag{3}$$

where $\boldsymbol{e}_\theta$ and $\boldsymbol{e}_\varphi$ are the unit vectors in the spherical coordinate system, and $E_{\theta n}$ and $E_{\varphi n}$ are the complex amplitude of the nth CEF in the far field along the θ-direction and φ-direction, respectively. Unless otherwise stated, the CEF mentioned in this article indicates the electric field in the far field. By analyzing the CEF, the far-field radiation of each mode can be investigated thoroughly. It is therefore feasible to calculate the total far-field radiation quantitatively, whereby the radiation of an antenna can be adjusted for specific applications such as the control of radiation null [23].

B. CMA of the SCS Without Excitation Units

The SCS under investigation with its geometrical dimensions is shown in Fig. 1. The CMs of the SCS are calculated by FEKO, and the eigenvalues of the first eight modes within 2–3 GHz are shown in Fig. 2. As shown, the eigenvalue magnitudes of Modes 1–4 are less than 3 within the interested frequency range (2.4–2.5 GHz). Modes 5–8 have

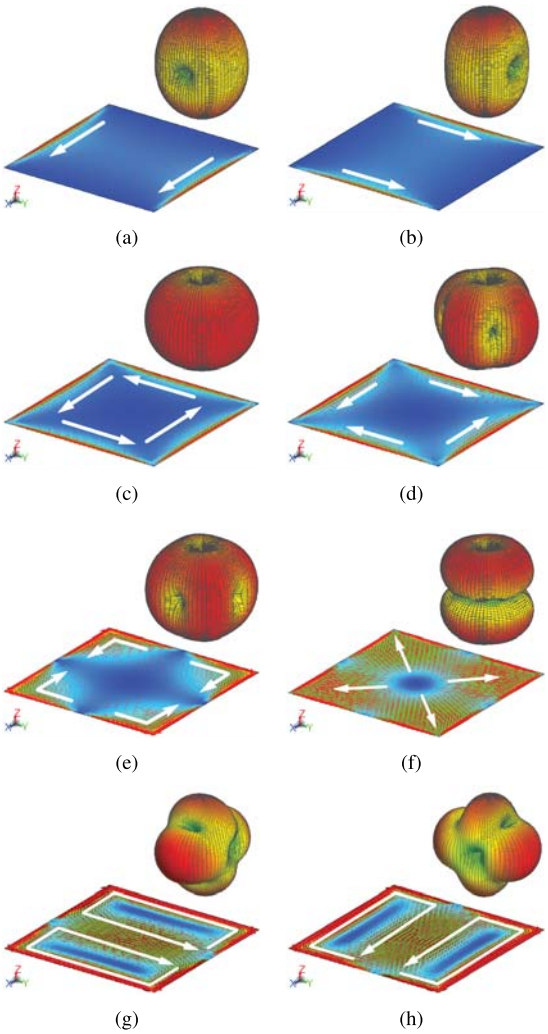

Fig. 3. Current mode distribution and the corresponding mode radiation pattern of the SCS at 2.45 GHz. (a) Mode 1. (b) Mode 2. (c) Mode 3. (d) Mode 4. (e) Mode 5. (f) Mode 6. (g) Mode 7. (h) Mode 8.

larger eigenvalue magnitudes and are regarded as high-order modes. Although these high-order modes are not constructive to impedance matching, they may benefit the radiation performance in terms of maintaining broadside radiation and low cross polarization.

To design an antenna with broadside radiation pattern, it is necessary to investigate the radiation performance of each mode. The current mode distribution $\boldsymbol{J}_n$ of the first eight modes and corresponding mode radiation pattern at 2.45 GHz are plotted in Fig. 3, where the white arrows indicate the current direction on the SCS. As can be seen, $\boldsymbol{J}_1$ is polarized in the x-direction, which hints that a pure x-direction polarized radiation can be obtained from Mode 1. The radiation pattern of Mode 1 is similar to that of a dipole for their analogous current distribution and thus is broadside directed. $\boldsymbol{J}_2$ is identical to $\boldsymbol{J}_1$ in magnitude but is polarized in the y-direction. Thus, $\boldsymbol{J}_1$ and $\boldsymbol{J}_2$ are a pair of orthogonal current modes and are good candidates for pure linearly polarized antennas. Besides, it is evident that $\boldsymbol{J}_7$ and $\boldsymbol{J}_8$ are another pair of orthogonal current modes with broadside radiation patterns. $\boldsymbol{J}_3$, $\boldsymbol{J}_4$, $\boldsymbol{J}_5$, and $\boldsymbol{J}_6$ all have a null radiation at boresight due to the antiphase

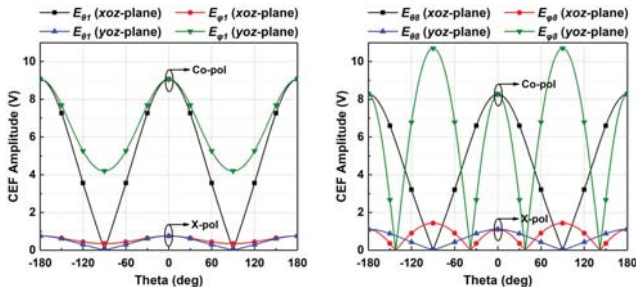

(a) (b)

Fig. 4. Amplitude of characteristic electric field at 2.45 GHz. (a) Mode 1. (b) Mode 8.

current distribution on the SCS. For achieving an antenna with broadside radiation pattern, $\boldsymbol{J}_1$, $\boldsymbol{J}_2$, $\boldsymbol{J}_7$, and $\boldsymbol{J}_8$ are thus chosen for further investigation.

Moreover, in order to obtain low cross polarization, the CEF needs to be investigated thoroughly. The CEFs of Modes 1 and 8 are shown in Fig. 4. From Fig. 4(a), it is shown that the co-polarization component of Mode 1 in xoz plane is θ-component, whereas φ-component in yoz plane. Both the θ-component in xoz plane and φ-component in yoz plane point to the x-direction at boresight, which verifies that Mode 1 is x-direction polarized. Similarly, Mode 8 is also x-direction polarized. In addition, it is noted that a large electric field amplitude ratio (EAR) between the co-polarization and cross polarization at boresight can be obtained under Modes 1 and 8. Specifically, the EAR is greater than 12 for Mode 1 and larger than 8 for Mode 8. Consequently, Modes 1 and 8 are applicable for realizing an x-direction polarized antenna with low cross polarization. Considering the symmetrical structure of the SCS, it is apparent that Modes 2 and 7 are also suitable for achieving low cross polarization. The only difference is that Modes 2 and 7 are y-direction polarized. For simplicity, Modes 1 and 8 are named VP modes for the polarization along the x-direction, whereas Modes 2 and 7 are called HP modes for the polarization along the y-direction.

C. CMA of the SCS With Four Groups of BIEs

Aiming at individually exciting VP modes or HP modes of the SCS and suppressing other destructive modes, the feeding structure should be designed elaborately. To this end, a novel excitation unit named BIE was utilized to excite modes selectively [33], which is also suitable for our design. As shown in Fig. 5(a), a BIE consists of two symmetric metallic semiloops with the left side shorted to the SCS and the feeding point located on the right side. Since the two semiloops are fed in-phase, the electric currents along the two loops are in the same direction, hence exciting two in-phase equivalent magnetic currents ($\boldsymbol{M}$). Attributed to these two in-phase equivalent magnetic currents, $\boldsymbol{J}_5$ and $\boldsymbol{J}_6$ can be restrained effectively for their out-of-phase current distribution at the edges of the SCS. To suppress $\boldsymbol{J}_3$ and $\boldsymbol{J}_4$, the two opposite BIEs are excited out of phase (notice that the opposite BIEs are arranged reversely) and the excitation configuration is shown in Fig. 5(b). By the way, the out-of-phase excitation in CMA is realized by the ideal wire ports and the voltage sources

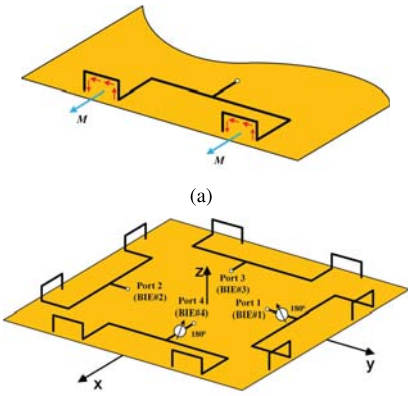

Fig. 5. BIEs arrangement over the SCS. (a) Two equivalent magnetic currents and a BIE. (b) Excitation configuration.

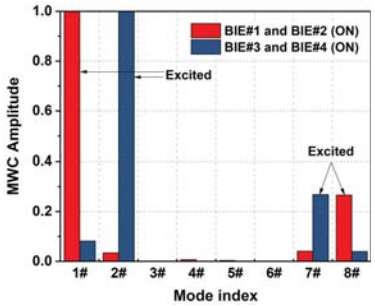

Fig. 6. Normalized MWC amplitude at 2.45 GHz when BIE#1 and BIE#2 or BIE#3 and BIE#4 are stimulated.

with adjustable phase, which are also used in [23] and [33]. With this feeding arrangement, the constructive Modes 1, 2, 7, and 8 can be excited effectively, while the unwanted Modes 3, 4, 5, and 6 are suppressed to a considerable extent.

It is worth pointing out that any modification of the investigated object affects the CMs by means of changing the eigenvalues and the current modes distribution over the object. Therefore, before demonstrating which modes have been stimulated by the BIEs, CMs for the new configuration (SCS + BIEs) need to be investigated. To avoid confusion, the nth CM of the new configuration is named Mode n#, and the corresponding current mode is denoted as $\boldsymbol{J}_{n\#}$.

To verify that the proposed feeding structure can excite the constructive modes and suppress the unwanted modes effectively, the normalized MWC amplitude of each mode at 2.45 GHz is evaluated in Fig. 6. As shown in Fig. 6, the normalized MWC amplitudes of all modes are less than 0.1 except for the VP modes (Modes 1 and 8) when BIE#1 and BIE#2 are stimulated simultaneously. When BIE#3 and BIE#4 are stimulated, only the HP modes (Modes 2 and 7) can be excited effectively. This also demonstrates the feasibility of selective excitation of the constructive modes by the BIEs.

The comparison between the SCS and the (SCS + BIEs) in terms of eigenvalues is shown in Fig. 7. The introduction of BIEs slightly changes the eigenvalues of the desired modes. From Fig. 8, it is observed that the current modes distribution and the mode radiation patterns of all the involved modes have no entitative variations except for the slight pattern rotation

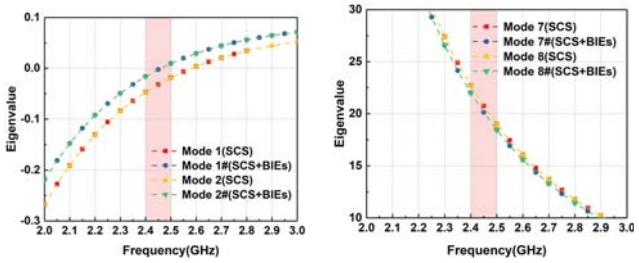

Fig. 7. Eigenvalues comparison. (a) Mode 1 versus Mode 1# and Mode 2 versus Mode 2#. (b) Mode 7 versus Mode 7# and Mode 8 versus Mode 8#.

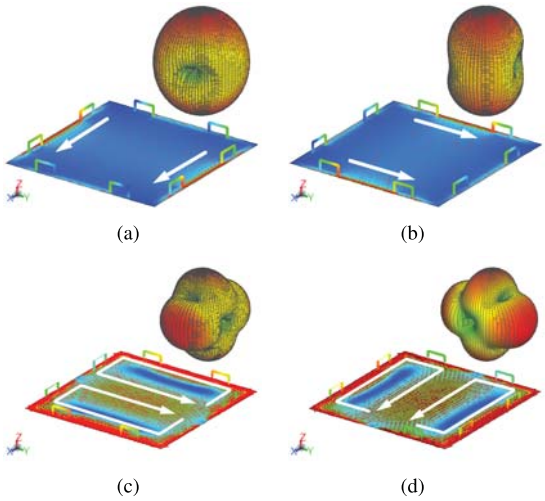

Fig. 8. Current mode distribution and the corresponding mode radiation pattern of SCS + BIEs at 2.45 GHz. (a) Mode 1#. (b) Mode 2#. (c) Mode 7#. (d) Mode 8#.

around the z-axis in Modes 1# and 2#. The desired modes still have broadside radiation patterns.

Considering the symmetry of the SCS and BIEs, the CEF variations of the VP modes and HP modes are consistent when the BIEs are introduced. For simplicity, only the variations of CEF under VP modes and the corresponding full-wave analysis are discussed in the following content. As shown in Fig. 9, compared to Mode 1, the cross-polarization components of Mode 1# in the two principal planes suffer from a fatal increase, which results in a low EAR. On the contrary, the EAR of Mode 8# has a slight improvement. From (3), when BIE#1 and BIE#2 are excited, the total electric field ($\boldsymbol{E}_{tot}^{(1,2)}$) in far field can be expressed as

$$\begin{aligned}\boldsymbol{E}_{tot} &= \sum_n \alpha_n \left(E_{\theta n}\,\boldsymbol{e}_\theta + E_{\varphi n}\,\boldsymbol{e}_\varphi\right)\\ &\cong \alpha_{1\#}^{(1,2)}\left(E_{\theta 1\#}\,\boldsymbol{e}_\theta + E_{\varphi 1\#}\,\boldsymbol{e}_\varphi\right)\\ &\quad + \alpha_{8\#}^{(1,2)}\left(E_{\theta 8\#}\,\boldsymbol{e}_\theta + E_{\varphi 8\#}\,\boldsymbol{e}_\varphi\right)\\ &= \left(\alpha_{1\#}^{(1,2)}\,E_{\theta 1\#} + \alpha_{8\#}^{(1,2)}\,E_{\theta 8\#}\right)\boldsymbol{e}_\theta\\ &\quad + \left(\alpha_{1\#}^{(1,2)}\,E_{\varphi 1\#} + \alpha_{8\#}^{(1,2)}\,E_{\varphi 8\#}\right)\boldsymbol{e}_\varphi \end{aligned} \tag{4}$$

where $\alpha_n^{(1,2)}$ is the MWC when BIE#1 and BIE#2 are stimulated simultaneously. In this case, the radiation performance of the antenna mainly depends on Modes 1# and 8#. Due to the deterioration of the cross-polarization performance in Mode 1#, exciting the VP modes directly will not obtain a

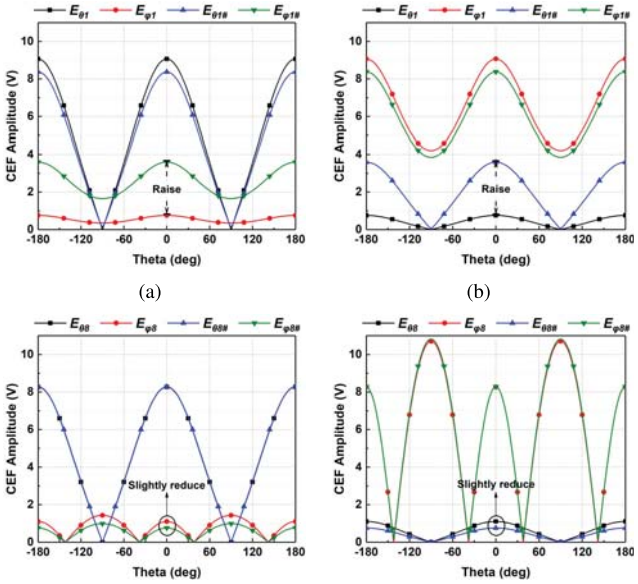

Fig. 9. Characteristic electric field amplitude comparison between SCS and SCS + BIEs at 2.45 GHz. (a) Mode 1 versus Mode 1# (*xoz* plane). (b) Mode 1 versus Mode 1# (*yoz* plane). (c) Mode 8 versus Mode 8# (*xoz* plane). (d) Mode 8 versus Mode 8# (*yoz* plane).

radiation pattern with low cross-polarization level in the two principal planes. To give a more intuitive understanding of the radiation performance of the proposed antenna when BIE#1 and BIE#2 are excited, the full-wave simulation patterns are shown in Fig. 10. As shown in Fig. 10, the simulated cross-polarization level is just around −10 dB at boresight.

D. Method of Cross-Polarization Suppression

As indicated earlier, the cross-polarization performance of the proposed antenna will deteriorate when the BIEs are used for mode excitation. In order to improve the cross-polarization performance, a novel method, which subtly introduces the co-polarization component of the orthogonal mode to counteract the cross-polarization component of the fundamental mode, is proposed. Considering the VP modes, orthogonal Mode 2# (HP mode) is introduced to reduce the cross polarization. From (4), the total electric field in far field after introducing the orthogonal mode (Mode 2#) changes to

$$\begin{aligned}\boldsymbol{E}_{tot} &\cong \alpha_{1\#}^{(1,2)}\boldsymbol{E}_{1\#}+\alpha_{2\#}^{(1,2)}\boldsymbol{E}_{2\#}+\alpha_{8\#}^{(1,2)}\boldsymbol{E}_{8\#}\\ &=\Big[\Big|\alpha_{1\#}^{(1,2)}\Big||E_{\theta 1\#}|\,e^{j(\gamma_{1\#}+\theta_{1\#})}+\Big|\alpha_{2\#}^{(1,2)}\Big||E_{\theta 2\#}|\,e^{j(\gamma_{2\#}+\theta_{2\#})}\\ &\quad+\Big|\alpha_{8\#}^{(1,2)}\Big||E_{\theta 8\#}|\,e^{j(\gamma_{8\#}+\theta_{8\#})}\Big]\boldsymbol{e}_{\theta}\\ &\quad+\Big[\Big|\alpha_{1\#}^{(1,2)}\Big||E_{\varphi 1\#}|\,e^{j(\gamma_{1\#}+\varphi_{1\#})}+\Big|\alpha_{2\#}^{(1,2)}\Big||E_{\varphi 2\#}|\,e^{j(\gamma_{2\#}+\varphi_{2\#})}\\ &\quad+\Big|\alpha_{8\#}^{(1,2)}\Big||E_{\varphi 8\#}|\,e^{j(\gamma_{8\#}+\varphi_{8\#})}\Big]\boldsymbol{e}_{\varphi}\end{aligned}\tag{5}$$

where $\gamma_{n\#}$ represents the phase of the nth mode's MWC and $\theta_{n\#}$ and $\varphi_{n\#}$ are the phase of the nth mode's CEF. To explain the proposed method in detail, the phase of the CEF of Modes 1# and 2# is investigated at first. As shown in Fig. 11, the phase difference of 180° between the co-polarization of Mode 1# and the cross polarization of Mode 2# is observed,

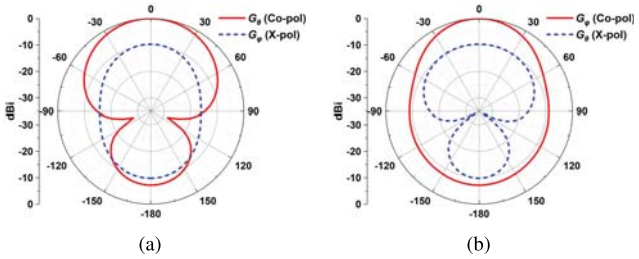

Fig. 10. Full-wave simulation patterns at 2.45 GHz when BIE#1 and BIE#2 are stimulated. (a) *xoz* plane. (b) *yoz* plane.

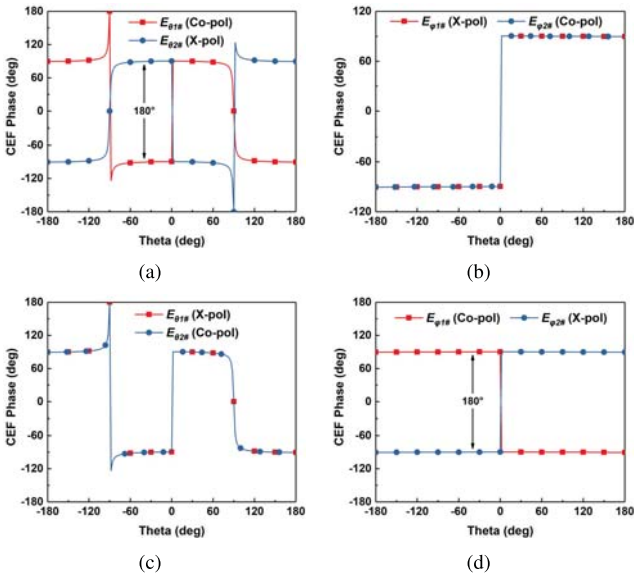

Fig. 11. Characteristic electric field phase comparison between Modes 1# and 2#. (a) θ-components (*xoz* plane). (b) φ-components (*xoz* plane). (c) θ-components (*yoz* plane). (d) φ-components (*yoz* plane).

whereas the cross polarization of Mode 1# and co-polarization of Mode 2# are in phase in both two principal planes. If the MWC of Modes 1# and 2# is out of phase ($\gamma_{2\#}-\gamma_{1\#}=\pi$), the cross-polarization component of Mode 1# can be canceled out by the co-polarization component of Mode 2#, that is

$$\begin{aligned}&in\ xoz\text{-}plane\begin{cases}\theta_{2\#}-\theta_{1\#}=\pi\\ \varphi_{2\#}=\varphi_{1\#}\\ \gamma_{2\#}-\gamma_{1\#}=\pi\end{cases}\\ &\Downarrow\\ &\begin{cases}(\gamma_{2\#}+\theta_{2\#})-(\gamma_{1\#}+\theta_{1\#})=0\\ (\gamma_{2\#}+\varphi_{2\#})-(\gamma_{1\#}+\varphi_{1\#})=\pi\end{cases}\end{aligned}\tag{6}$$

$$\begin{aligned}&in\ yoz\text{-}plane\begin{cases}\theta_{1\#}=\theta_{2\#}\\ \varphi_{1\#}-\varphi_{2\#}=\pi\\ \gamma_{2\#}-\gamma_{1\#}=\pi\end{cases}\\ &\Downarrow\\ &\begin{cases}(\gamma_{2\#}+\theta_{2\#})-(\gamma_{1\#}+\theta_{1\#})=\pi\\ (\gamma_{2\#}+\varphi_{2\#})-(\gamma_{1\#}+\varphi_{1\#})=0.\end{cases}\end{aligned}\tag{7}$$

For VP modes, the co-polarization component (θ-component) in the *xoz* plane is thus superposed in-phase, whereas the cross-polarization component (φ-component) is greatly suppressed. Likewise, in the *yoz* plane, the co-polarization component (φ-component) is enhanced, whereas the

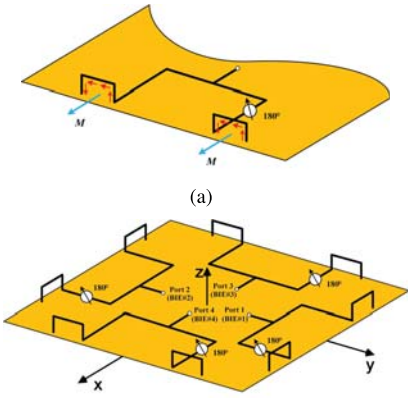

(a)

(b)

Fig. 12. Modified feeding strategy. (a) Modified BIE. (b) Modified excitation configuration.

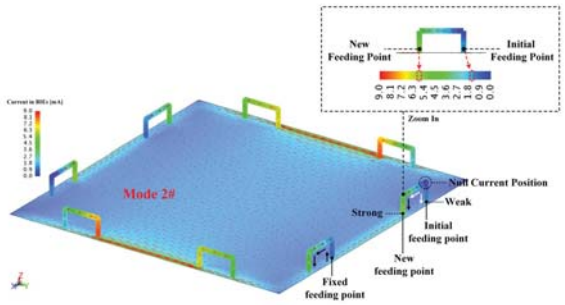

(a)

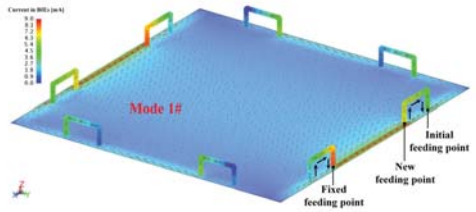

(b)

Fig. 13. Current mode distribution at 2.45 GHz. (a) Mode 2#. (b) Mode 1#.

cross-polarization component (θ-component) is greatly reduced.

Based on this idea, two modifications are made to the feeding strategy. As shown in Fig. 12(a), the first alteration is moving the feeding point from the right side to the inner side of the two semiloops. Besides, an additional phase shift of 180° is added into one of the two semiloops to generate the in-phase magnetic current. Another change is that all ports are fed in phase. The final excitation configuration is shown in Fig. 12(b). It is worth mentioning that these alterations do not change the antenna geometry and are realized by using wire ports and voltages sources similar to the method used in [23] and [33]. Consequently, the CMs analyzed earlier are still available and the CEF does not change under the modified feeding configuration. For the purpose of giving an

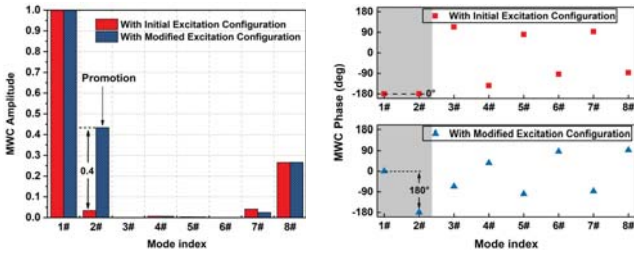

(a) (b)

Fig. 14. Normalized MWC when BIE#1 and BIE#2 are stimulated at 2.45 GHz. (a) Normalized MWC amplitude. (b) MWC phase.

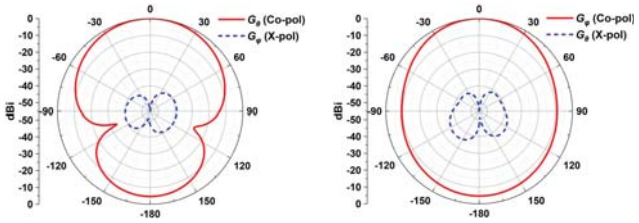

(a) (b)

Fig. 15. Full-wave simulation normalized radiation patterns with modified feeding strategy at 2.45 GHz when BIE#1 and BIE#2 are stimulated. (a) *xoz* plane. (b) *yoz* plane.

intuitive explanation about how Mode 2# is introduced, the detailed analysis for Modes 1# and 2# is shown in Fig. 13. The black and white solid arrows in Fig. 13 both indicate the direction of the characteristic current along BIEs. Focusing on the BIE#1, it is observed from Fig. 13(a) that the characteristic current density of Mode 2# nearby the new feeding point is stronger than that around the initial feeding point. Moving the feeding point from the initial one to the new one, the modal excitation coefficient of Mode 2# ($V^i_{2\#}$) would be increased prominently, leading to the promotion of MWC amplitude of Mode 2#. Besides, the variation of the feeding phase makes the $V^i_{2\#}$ in-phase at each port, which further enhances the MWC amplitude of Mode 2#. Fig. 14(a) confirms that prominent promotion of the MWC amplitude of Mode 2# is realized compared with the initial feeding configuration.

On the other hand, it is noted that a null of $\boldsymbol{J}_{2\#}$ occurs at one semiloop of the BIE#1, which means that the direction of $\boldsymbol{J}_{2\#}$ at this position will be inversed. Here, white solid arrows are used to highlight this phenomenon. Under the modified feeding strategy, the direction of $\boldsymbol{J}_{2\#}$ is opposite to the direction of $\boldsymbol{J}_{1\#}$ at both the fixed feeding point and the new feeding point. Since the feeding phase is the same for the two modes, the phase of $V^i_{2\#}$ is of 180° difference to the phase of $V^i_{1\#}$ according to (2). Consequently, 180° difference between the MWC phases of Modes 1# and 2# is realized by the modified BIE#1. The same analysis is also applicable to BIE#2. Fig. 14(b) clearly shows that the MWC of Modes 1# and 2# is in phase with the initial excitation configuration and out-of-phase with the modified excitation configuration.

In order to verify the effectiveness of the proposed method in cross-polarization suppression, full-wave simulated radiation patterns are shown in Fig. 15. As shown, remarkable cross-polarization performance is achieved and the cross polarization is greatly suppressed from −10 to −40 dB. Likewise,

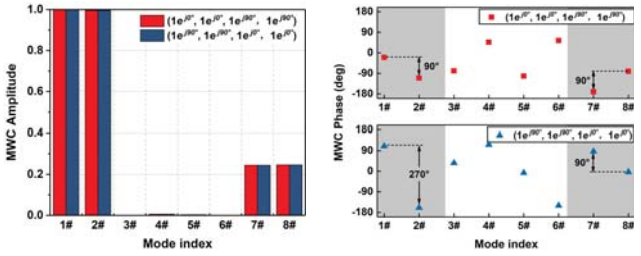

(a) (b)

Fig. 16. Normalized MWC amplitude and the MWC phase at 2.45 GHz. (a) Normalized MWC amplitude. (b) MWC phase.

the proposed method is also applicable for reducing the cross polarization of the HP modes when BIE3# and BIE4# are ON. Compared with the method used to suppress the cross polarization in [34] and [35], the proposed method is different due to the following reasons. First, two orthogonal current modes instead of two oppositely directed currents employed in [34] and [35] are used to suppress the cross polarization. Besides, in the proposed method, the co-polar component of the orthogonal mode is promoted intentionally to cancel out the cross-polar component of the fundamental mode. However, the cross-polar component is canceled due to the differential feeding in [34] and [35], which has nothing to do with the co-polar fields. Moreover, the feeding phase is actually the same for the fundamental mode and orthogonal mode, which is also different from the differential feeding in [34] and [35].

III. Implementation of Quad-Polarization Reconfiguration

A. Capability of Circular Polarization Operation

As aforementioned, two orthogonal linear polarizations with low cross polarization in the two principal planes can be realized by stimulating the BIEs along the x- or y-axes, respectively. Consequently, once a phase difference of 90° is introduced and the equal amplitude is maintained between the VP and HP modes, the circular polarization can be achieved. In order to validate this assumption, two groups of feeding states for the four ports are designed and denoted as ($A_1e^{j\phi_1}$, $A_2e^{j\phi_2}$, $A_3e^{j\phi_3}$, and $A_4e^{j\phi_4}$), where A_n and ϕ_n represent the feeding amplitude and feeding phase of the corresponding port, respectively. The normalized MWC amplitude and MWC phase of the two different feeding states are shown in Fig. 16. As can be seen, the VP modes and HP modes are excited in equal amplitude under both feeding states. Meanwhile, it can be seen from Fig. 16(b) that the phase difference of 90° is realized between the VP modes and HP modes. When the feeding state is ($1e^{j0^\circ}$, $1e^{j0^\circ}$, $1e^{j90^\circ}$, and $1e^{j90^\circ}$), the MWC phase of VP modes lags behind HP modes by 90°. For the state of ($1e^{j90^\circ}$, $1e^{j90^\circ}$, $1e^{j0^\circ}$, and $1e^{j0^\circ}$), the MWC phase of VP modes leads HP modes by 90°. These results prove that the equal MWC amplitude and the quadrature phase difference between the VP modes and HP modes can be realized by choosing appropriate feeding signals. In Fig. 17, the corresponding full-wave simulation results verify that RHCP and LHCP radiation patterns are realized with a good cross-polarization performance.

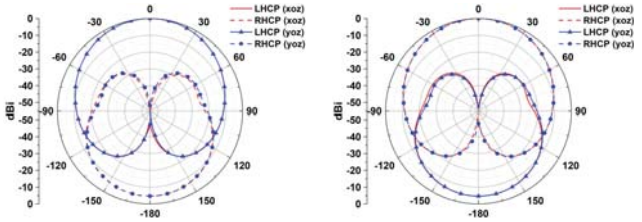

(a) (b)

Fig. 17. Full-wave simulated normalized radiation patterns at 2.45 GHz. (a) LHCP ($1e^{j0^\circ}$, $1e^{j0^\circ}$, $1e^{j90^\circ}$, and $1e^{j90^\circ}$). (b) RHCP ($1e^{j90^\circ}$, $1e^{j90^\circ}$, $1e^{j0^\circ}$, and $1e^{j0^\circ}$).

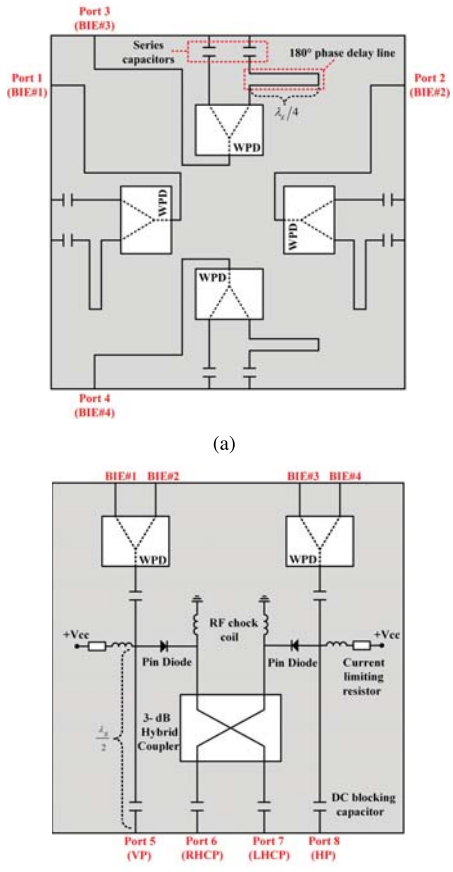

(a)

(b)

Fig. 18. Feeding network schematic diagrams. (a) Feeding network I: series capacitor $C = 0.2$ pF. (b) Feeding network II: RF choke coil $L_1 = 22$ nH, DC blocking capacitor $C_1 = 1000$ pF, and current-limiting resistor $R_1 = 82\ \Omega$.

B. Implementation of Quad-Polarization Reconfiguration

As indicated earlier, the methods to stimulate the VP, HP, LHCP, and RHCP radiation with low cross polarization in the two principal planes are illustrated separately. A quad-polarization reconfigurable antenna is thus conceived in such a way that its capability of polarization reconfiguration can be realized by a reconfigurable feeding network. To this end, an elaborated feeding network is designed and its schematics with detailed parameters are shown in Fig. 18. Due to the limited size of the SCS, the entire feeding network cannot be fully printed on the back side of the SCS, and thus, is divided into two parts, namely, feeding networks I and II.

TABLE I
INPUT PORTS AND THE CORRESPONDING POLARIZATION STATES

State	Input Port	PIN Diodes	BIE#1 and BIE#2	BIE#3 and BIE#4	Polarization
State 1	Port 5	Off	Enabled	Disabled	VP
State 2	Port 6	On	Enabled(90°)	Enabled(0°)	RHCP
State 3	Port 7	On	Enabled(0°)	Enabled(90°)	LHCP
State 4	Port 8	Off	Disabled	Enabled	HP

(a) (b)

Fig. 19. Equivalent circuit for the p-i-n diode. (a) Forward bias. (b) Reverse bias. L_s = 0.6 nH, $R_s = 2.1\ \Omega$, $C_T = 0.17$ pF, and $R_p = 5$ kΩ.

As shown in Fig. 18(a), feeding network I is composed of four Wilkinson power dividers (WPDs), four half-wavelength delay lines, and eight lumped capacitors. The WPD and delay line are mainly used to implement the BIE excitations. In addition, eight lumped capacitors are embedded to neutralize the imaginary part of input impedance introduced by Modes 7# and 8# (inductive mode). Fig. 18(b) shows feeding network II that is composed of two WPDs, two p-i-n diodes, as well as a quadrature hybrid coupler. The WPDs in feeding network II are adopted to split the input signal into two output signals with equal magnitude. The quadrature hybrid coupler is employed to implement the 90° phase shift between (BIE#1 and BIE#2) and (BIE#3 and BIE#4). By switching the ON/OFF states of the p-i-n diodes, the polarization of the proposed antenna can be changed. It is worth pointing out that the four inputs in feeding network II can be merged into one port. However, additional p-i-n diodes and bias circuits are required to achieve this, which inevitably increases the insertion loss and design complexity of the feeding network. The corresponding equivalent circuit of the two p-i-n diodes is shown in Fig. 19. When port 5 is turned on and the two p-i-n diodes are all OFF, BIE#1 and BIE#2 are enabled, whereas BIE#3 and BIE#4 are disabled, leading to a VP radiation. When port 6 is excited and the two p-i-n diodes are all ON, the four BIEs are enabled, but there is 90° phase shift between (BIE#1 and BIE#2) and (BIE#3 and BIE#4). Hence, the RHCP radiation is achieved. In summary, all the antenna operation states are listed in Table I.

IV. RESULTS AND DISCUSSION

To verify the design concept, the radiator and the feeding network are fabricated on two FR-4 substrates, both with a size of 65 mm × 65 mm. The permittivity of the substrate is 4.2 and its thickness is 0.6 mm. According to [36], the introduction of a substrate shows a limited effect on the CMs

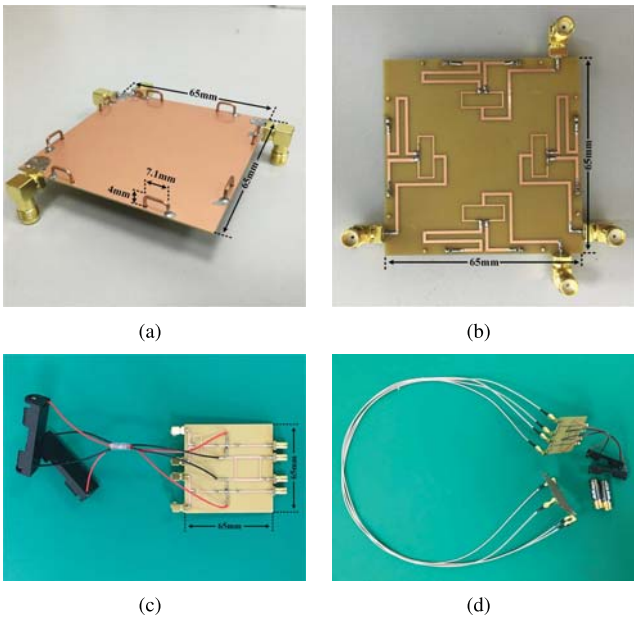

(a) (b)

(c) (d)

Fig. 20. Fabricated prototype of the antenna system. (a) SCS with four groups of BIEs. (b) Feeding network I. (c) Feeding network II. (d) Overall antenna system.

analyzed in Section II. Fig. 20 shows the fabricated prototypes. As shown in Fig. 20(a), the SCS is printed on the top layer of the substrate with four BIEs located at the edges of the slab. To make the real part of the input impedance close to 50 Ω, the geometry dimensions and the location of each semiloop exciter are optimized. In detail, each semiloop exciter is bent from a copper rod with a radius of 0.5 mm. The length and height of the semiloop exciter are 7.1 and 4 mm, respectively. The distance between two neighboring semiloop exciters is 24.5 mm. Besides, each BIE is of 2 mm distance to the edge of the board. As shown in Fig. 20(b), feeding network I is printed on the back of the SCS for reducing the fabrication complexity. From Fig. 20(c), it is shown that feeding network II is printed on another substrate. The two p-i-n diodes (Infineon BAR64-02) in feeding network II are driven by two batteries with 1.5-V DC voltages. Fig. 20(d) shows that the two separated parts are connected by four 50 Ω coaxial cables with equal phases.

A. Performance of Radiator With Feeding Network I

The comparison between the simulated and measured reflection coefficients (S_{ii}) of the proposed antenna with feeding

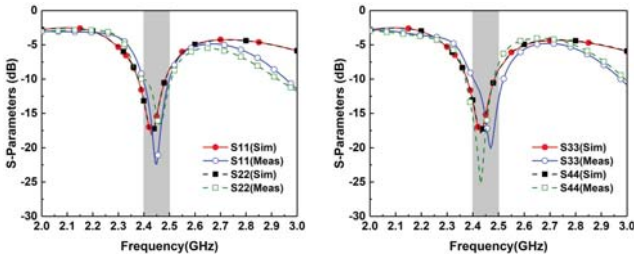

Fig. 21. Comparison between the simulated and measured S_{ii} with feeding network I. (a) S_{11} and S_{22}. (b) S_{33} and S_{44}.

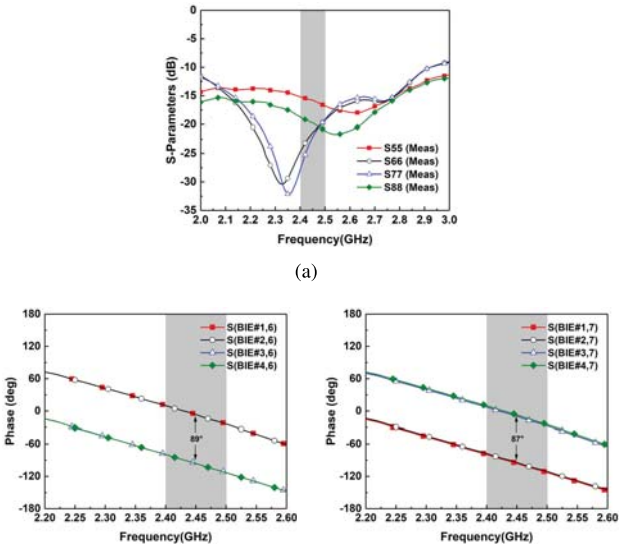

Fig. 22. Measured S-parameters of feeding network II. (a) S-parameters. (b) Phase of $S(i,6)$. (c) Phase of $S(i,7)$.

network I is shown in Fig. 21. Good agreement between the simulation and measurement results is observed. There is a small frequency shift with respect to the simulation results, which may attribute to the fabrication errors of the semiloop exciters and the misalignment between the two semiloop exciters. Nevertheless, the proposed antenna fed through feeding network I demonstrates a good impedance matching within the interested frequency band (2.4–2.5 GHz).

B. Performance of Feeding Network II

As the performance of the feeding network II affects the overall antenna performance, it should be investigated separately. The measured S-parameters of the feeding network II are shown in Fig. 22. The reflection coefficient (S_{ii}) of all input ports is less than −10 dB within the operating frequency range. As shown in Fig. 22(b) and (c), around 90° phase shift is realized by the quadrature hybrid coupler when port 6 or port 7 is excited, which ensures the implementation of the circular polarization operation.

C. Performance of Overall Antenna System

To provide a fair comparison, the simulated reflection coefficient of the overall antenna system is provided and denoted as S_{ii} combined (Sim). It is worth pointing out that the cables are also included in the simulation, and thus, the fluctuation is observed in the simulated reflection coefficients. The simulated and measured overall S-parameters are plotted in Fig. 23, which both indicate a good impedance matching from 2.4 to 2.5 GHz. As can be seen from Figs. 21 and 23, the reflection coefficients are reduced in the overall antenna system, leading to an illusion of expanded bandwidth. It is necessary to explain that the reflection coefficients lower than −10 dB outside the operating bandwidth region are mainly caused by the loss of the coaxial cables.

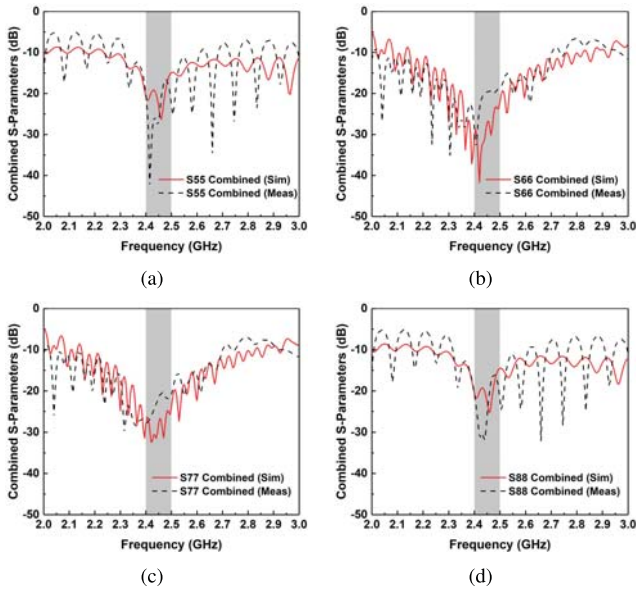

Fig. 23. Comparison between the simulated and measured overall S-parameters. (a) S_{55}. (b) S_{66}. (c) S_{77}. (d) S_{88}.

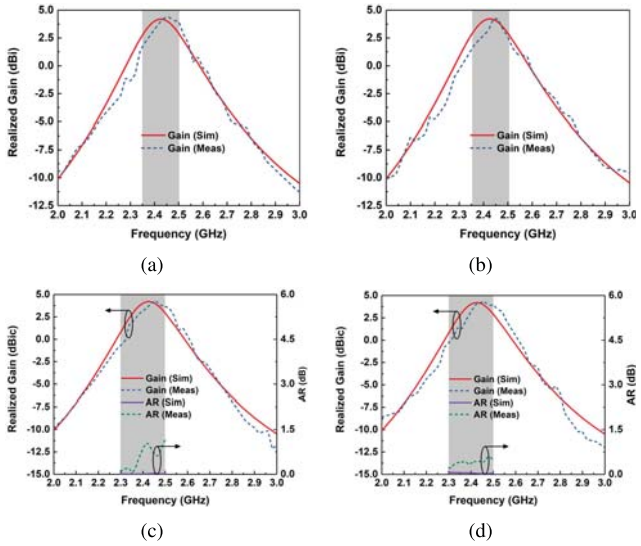

Fig. 24. Measured and simulated gains and ARs of the four different polarizations. (a) VP. (b) HP. (c) LHCP. (d) RHCP.

Fig. 24 shows the measured gains and the axial ratios (ARs) of the proposed antenna. The maximum measured gains are 4.22 dBi, 4.21 dBi, 4.26 dBic, and 4.29 dBic for VP, HP, LHCP, and RHCP, respectively. Discrepancies between the

TABLE II
PERFORMANCE COMPARISON OF POLARIZATION RECONFIGURABLE ANTENNAS

Ref.	Bandwidth	No. of Polarizations	Feeding Network	No. of Switches	No. of Ports	Cross Polarization	Design Method
[1]	3.55%	2 LP, 2CP	No	8 PIN Diodes	1	< -15 dB	ME Dipole Theory
[2]	1.06%	2 LP, 2CP	No	6 PIN Diodes	1	< -15 dB	/
[6]	7.03%	4 LP	No	4 PIN Diodes	1	< -10 dB	/
[7]	33.9%	1 LP, 2 CP	No	4 PIN Diodes	1	< -18 dB	ME Dipole Theory
[12]	15.9%	1 LP, 2 CP	No	3 PIN Diodes	1	< -18 dB	/
[14]	84.5%	2 LP, 2CP	Yes	8 PIN Diodes	1	< -18 dB	/
[30]	8.33%	1 LP, 2CP	Yes	2 PIN Diodes	1	< -20 dB	Characteristic Mode Theory
This work	4.08%	2 LP, 2CP	Yes	2 PIN Diodes	4	< -30 dB	Characteristic Mode Theory

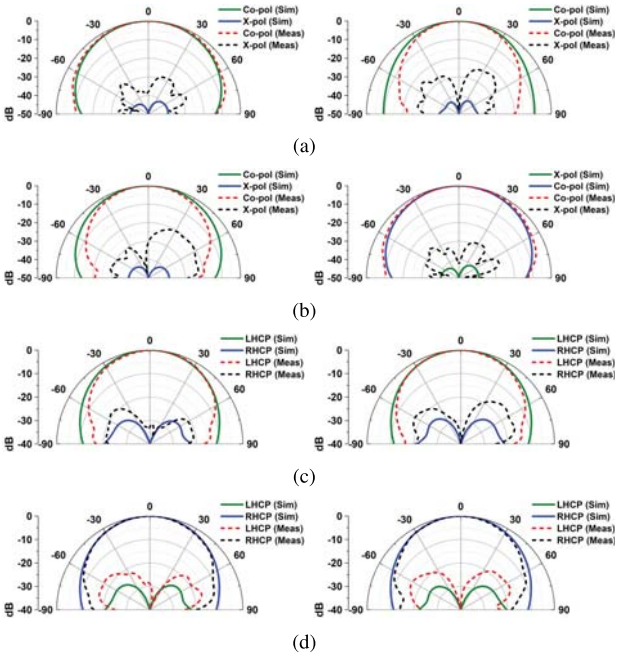

Fig. 25. Measured and simulated patterns in the *xoz* plane (left) and the *yoz* plane (right) under different polarizations. (a) VP. (b) HP. (c) LHCP. (d) RHCP.

simulated and measured ARs is due to the fact that ideal feeding ports are used in simulation. In spite of this, the ARs for LHCP and RHCP are both lower than 1.5 dB, which indicates the good circular polarization performance of the proposed antenna.

The simulated and measured normalized radiation patterns in the two principal planes (*xoz* and *yoz* planes) are presented in Fig. 25. The measured cross-polarization levels are all lower than −30 dB at boresight. The rise of the measured cross-polarization level is due to the limitation of the measurement facilities. The measurement results verify that the proposed antenna can handle a quad-polarization operation and keep a low cross polarization in the two principal planes simultaneously.

To demonstrate the merits of the proposed antenna, comparisons between the proposed antenna and other polarization reconfigurable antennas are given in Table II. From Table II, it can be seen that the proposed antenna achieves full polarization agility by using two p-i-n diodes and four ports. Moreover, attributed to the presented method based on CMT, the proposed antenna exhibits better cross-polarization performance than other relevant works. Although the bandwidth of the proposed antenna is relatively narrow, the proposed method achieving low cross polarization can be operated over a much wider bandwidth. The reason for the limited antenna bandwidth is mainly due to the small electric size of the BIEs at 2.45 GHz, which needs an external matching circuit to achieve impedance matching and results in a narrowband performance [37], [38].

V. CONCLUSION

A novel method to suppress the cross polarization has been proposed and successfully implemented in a quad-polarization reconfigurable antenna. Detailed CMA of the whole radiating structure is conducted to explain the proposed method. From the analysis of a pair of orthogonal CMs, it is found that the cross-polarization component of the fundamental mode can be counteracted by the co-polarization component of the orthogonal mode, achieving a low cross polarization in the two principal planes. Four groups of BIEs are used to excite the constructive modes with desired phase differences, which helps realize a low cross polarization. By employing a reconfigurable feeding network with two p-i-n diodes, a quad-polarization reconfigurable antenna is implemented. Both simulated and measured results confirm that the proposed antenna achieves quad-polarization agility and a cross-polarization level lower than −30 dB in the two principal planes under all polarization states. The proposed method is believed to be applicable to other applications, such as the dynamic control of the AR beamwidth (ARBW) and the AR value for a circularly polarized antenna, and the suppression of cross polarization for other types of antennas.

REFERENCES

[1] F. Wu and K. M. Luk, "Single-port reconfigurable magneto-electric dipole antenna with quad-polarization diversity," *IEEE Trans. Antennas Propag.*, vol. 65, no. 5, pp. 2289–2296, May 2017.

[2] M.-C. Tang, Z. Wu, T. Shi, and R. W. Ziolkowski, "Electrically small, low-profile, planar, huygens dipole antenna with quad-polarization diversity," *IEEE Trans. Antennas Propag.*, vol. 66, no. 12, pp. 6772–6780, Dec. 2018.
[3] R. K. Singh, A. Basu, and S. K. Koul, "A novel reconfigurable microstrip patch antenna with polarization agility in two switchable frequency bands," *IEEE Trans. Antennas Propag.*, vol. 66, no. 10, pp. 5608–5613, Oct. 2018.
[4] J. Hu and Z. Hao, "Design of a frequency and polarization reconfigurable patch antenna with a stable gain," *IEEE Access*, vol. 6, pp. 68169–68175, 2018.
[5] K. M. Mak, H. W. Lai, K. M. Luk, and K. L. Ho, "Polarization reconfigurable circular patch antenna with a C-shaped," *IEEE Trans. Antennas Propag.*, vol. 65, no. 3, pp. 1388–1392, Mar. 2017.
[6] S.-L. Chen, F. Wei, P.-Y. Qin, Y. J. Guo, and X. Chen, "A multi-linear polarization reconfigurable unidirectional patch antenna," *IEEE Trans. Antennas Propag.*, vol. 65, no. 8, pp. 4299–4304, Aug. 2017.
[7] Y. Shi, Y. Cai, X.-F. Zhang, and K. Kang, "A simple tri-polarization reconfigurable magneto-electric dipole antenna," *IEEE Antennas Wireless Propag. Lett.*, vol. 17, no. 2, pp. 291–294, Feb. 2018.
[8] H. H. Tran, N. Nguyen-Trong, T. T. Le, and H. C. Park, "Wideband and multipolarization reconfigurable crossed bowtie dipole antenna," *IEEE Trans. Antennas Propag.*, vol. 65, no. 12, pp. 6968–6975, Dec. 2017.
[9] P. Kumar, S. Dwari, R. K. Saini, and M. K. Mandal, "Dual-band dual-sense polarization reconfigurable circularly polarized antenna," *IEEE Antennas Wireless Propag. Lett.*, vol. 18, no. 1, pp. 64–68, Jan. 2019.
[10] S. W. Lee and Y. J. Sung, "Simple polarization-reconfigurable antenna with T-shaped feed," *IEEE Antennas Wireless Propag. Lett.*, vol. 15, pp. 114–117, 2016.
[11] I. T. Mcmichael, "A mechanically reconfigurable patch antenna with polarization diversity," *IEEE Antennas Wireless Propag. Lett.*, vol. 17, no. 7, pp. 1186–1189, Jul. 2018.
[12] K. X. Wang and H. Wong, "A reconfigurable CP/LP antenna with cross-probe feed," *IEEE Antennas Wireless Propag. Lett.*, vol. 16, pp. 669–672, 2017.
[13] H. Sun and S. Sun, "A novel reconfigurable feeding network for quad-polarization-agile antenna design," *IEEE Trans. Antennas Propag.*, vol. 64, no. 1, pp. 311–316, Jan. 2016.
[14] X. Ding, Z. Zhao, Y. Yang, Z. Nie, and Q. H. Liu, "Wideband quad-polarization reconfigurable antenna using switchable feed network with stable unidirectional radiation patterns," *IEEE Access*, vol. 6, pp. 73434–73443, 2018.
[15] C. Ni, M. S. Chen, Z. X. Zhang, and X. L. Wu, "Design of frequency-and polarization-reconfigurable antenna based on the polarization conversion metasurface," *IEEE Antennas Wireless Propag. Lett.*, vol. 17, no. 1, pp. 78–81, Jan. 2018.
[16] H. L. Zhu, S. W. Cheung, X. H. Liu, and T. I. Yuk, "Design of polarization reconfigurable antenna using metasurface," *IEEE Trans. Antennas Propag.*, vol. 62, no. 6, pp. 2891–2898, Jun. 2014.
[17] Y. Chen and C. Wang, *Characteristic Mode Theory for PEC Bodies*. Hoboken, NJ, USA: Wiley, 2015.
[18] M. Cabedo-Fabres, E. Antonino-Daviu, A. Valero-Nogueira, and M. Bataller, "The theory of characteristic modes revisited: A contribution to the design of antennas for modern applications," *IEEE Antennas Propag. Mag.*, vol. 49, no. 5, pp. 52–68, Oct. 2007.
[19] E. Antonino-Daviu, M. Cabedo-Fabres, M. Sonkki, N. Mohamed Mohamed-Hicho, and M. Ferrando-Bataller, "Design guidelines for the excitation of characteristic modes in slotted planar structures," *IEEE Trans. Antennas Propag.*, vol. 64, no. 12, pp. 5020–5029, Dec. 2016.
[20] Q. Wu, "Characteristic mode assisted design of dielectric resonator antennas with feedings," *IEEE Trans. Antennas Propag.*, vol. 67, no. 8, pp. 5294–5304, Aug. 2019.
[21] N. L. Bohannon and J. T. Bernhard, "Design guidelines using characteristic mode theory for improving the bandwidth of PIFAs," *IEEE Trans. Antennas Propag.*, vol. 63, no. 2, pp. 459–465, Feb. 2015.
[22] T. Li and Z. N. Chen, "A dual-band metasurface antenna using characteristic mode analysis," *IEEE Trans. Antennas Propag.*, vol. 66, no. 10, pp. 5620–5624, Oct. 2018.
[23] F. A. Dicandia, S. Genovesi, and A. Monorchio, "Advantageous exploitation of characteristic modes analysis for the design of 3-D null-scanning antennas," *IEEE Trans. Antennas Propag.*, vol. 65, no. 8, pp. 3924–3934, Aug. 2017.
[24] F. H. Lin and Z. N. Chen, "Low-profile wideband metasurface antennas using characteristic mode analysis," *IEEE Trans. Antennas Propag.*, vol. 65, no. 4, pp. 1706–1713, Apr. 2017.
[25] Q. Zhang, R. Ma, W. Su, and Y. Gao, "Design of a multimode UWB antenna using characteristic mode analysis," *IEEE Trans. Antennas Propag.*, vol. 66, no. 7, pp. 3712–3717, Jul. 2018.
[26] Z. Miers, H. Li, and B. K. Lau, "Design of bandwidth-enhanced and multiband MIMO antennas using characteristic modes," *IEEE Antennas Wireless Propag. Lett.*, vol. 12, pp. 1696–1699, 2013.
[27] D. Manteuffel and R. Martens, "Compact multimode multielement antenna for indoor UWB massive MIMO," *IEEE Trans. Antennas Propag.*, vol. 64, no. 7, pp. 2689–2697, Jul. 2016.
[28] B. Yang and J. J. Adams, "Systematic shape optimization of symmetric MIMO antennas using characteristic modes," *IEEE Trans. Antennas Propag.*, vol. 64, no. 7, pp. 2668–2678, Jul. 2016.
[29] C. Deng, Z. Feng, and S. V. Hum, "MIMO mobile handset antenna merging characteristic modes for increased bandwidth," *IEEE Trans. Antennas Propag.*, vol. 64, no. 7, pp. 2660–2667, Jul. 2016.
[30] K. Li, Y. Shi, H. Shen, and L. Li, "A characteristic-mode-based polarization-reconfigurable antenna and its array," *IEEE Access*, vol. 6, pp. 64587–64595, 2018.
[31] B. Li, Y.-Z. Yin, W. Hu, Y. Ding, and Y. Zhao, "Wideband dual-polarized patch antenna with low cross polarization and high isolation," *IEEE Antennas Wireless Propag. Lett.*, vol. 11, pp. 427–430, 2012.
[32] J. J. H. Wang, "Antennas for global navigation satellite system (GNSS)," *Proc. IEEE*, vol. 100, no. 7, pp. 2349–2355, Jul. 2012.
[33] F. A. Dicandia, S. Genovesi, and A. Monorchio, "Efficient excitation of characteristic modes for radiation pattern control by using a novel balanced inductive coupling element," *IEEE Trans. Antennas Propag.*, vol. 66, no. 3, pp. 1102–1113, Mar. 2018.
[34] T.-W. Chiou and K.-L. Wong, "Broad-band dual-polarized single microstrip patch antenna with high isolation and low cross polarization," *IEEE Trans. Antennas Propag.*, vol. 50, no. 3, pp. 399–401, Mar. 2002.
[35] H. Wong, K. L. Lau, and K. M. Luk, "Design of dual-polarized L-probe patch antenna arrays with high isolation," *IEEE Trans. Antennas Propag.*, vol. 52, no. 1, pp. 45–52, Jan. 2004.
[36] H. Li, Z. T. Miers, and B. K. Lau, "Design of orthogonal MIMO handset antennas based on characteristic mode manipulation at frequency bands below 1 GHz," *IEEE Trans. Antennas Propag.*, vol. 62, no. 5, pp. 2756–2766, May 2014.
[37] R. Martens, E. Safin, and D. Manteuffel, "Inductive and capacitive excitation of the characteristic modes of small terminals," in *Proc. Loughborough Antennas Propag. Conf.*, Nov. 2011, pp. 1–7.
[38] R. Valkonen, A. Lehtovuori, and D. Manteuffel, "Capacitive coupling elements—Changing the way of designing antennas," in *Proc. 8th Eur. Conf. Antennas Propag.*, Apr. 2014, pp. 229–233.

Long Zhang (Member, IEEE) received the B.S. and M.S. degrees in electrical engineering from the Huazhong University of Science and Technology (HUST), Wuhan, China, in 2009 and 2012, respectively, and the Ph.D. degree in electronic engineering from the University of Kent, Canterbury, U.K, in 2017.

From January 2018 to April 2018, he was a Research Fellow with the Poly-Grames Research Center, Polytechnique Montreal, Montreal, QC, Canada. He is currently an Assistant Professor with the College of Electronics and Information Engineering, Shenzhen University, Shenzhen, China. His current research interests include circularly polarized antennas and arrays, millimeter-wave antennas and arrays, tightly coupled arrays, reflectarrays, and characteristic mode theory.

Dr. Zhang has served as a TPC member and the session chair for several international conferences. He was a recipient of the Shenzhen Overseas High-Caliber Personnel Level C ("Peacock Plan Award" C). He also serves as a Reviewer for several technique journals, including the IEEE TRANSACTIONS ON ANTENNAS AND PROPAGATION and the IEEE ANTENNAS AND WIRELESS PROPAGATION LETTERS.

Yuhang Sun received the B.S. and M.S. degrees from the College of Electronics and Information Engineering, Shenzhen University, Shenzhen, Guangdong, China, in 2017 and 2020, respectively.

His current research interests include reconfigurable antennas, circularly polarized antennas, and characteristic mode theory.

Yejun He (Senior Member, IEEE) received the Ph.D. degree in information and communication engineering from the Huazhong University of Science and Technology (HUST), Wuhan, China, in 2005.

From 2005 to 2006, he was a Research Associate with the Department of Electronic and Information Engineering, The Hong Kong Polytechnic University, Hong Kong. From 2006 to 2007, he was a Research Associate with the Department of Electronic Engineering, Faculty of Engineering, The Chinese University of Hong Kong, Hong Kong. In 2012, he was a Visiting Professor with the Department of Electrical and Computer Engineering, University of Waterloo, Waterloo, ON, Canada. From 2013 to 2015, he was an Advanced Visiting Scholar (Visiting Professor) with the School of Electrical and Computer Engineering, Georgia Institute of Technology, Atlanta, GA, USA. He has been a Full Professor with the College of Electronics and Information Engineering, Shenzhen University, Shenzhen, China, where he is currently the Director of the Guangdong Engineering Research Center of Base Station Antennas and Propagation and the Director of the Shenzhen Key Laboratory of Antennas and Propagation. He has authored or coauthored more than 180 research articles and books (chapters). He holds about 20 patents. He has served as the General Chair of the IEEE ComComAp 2019. His research interests include wireless communications, antennas, and radio frequency.

Dr. He is a fellow of the Institution of Engineering and Technology and the Chair of the IEEE Antennas and Propagation Society-Shenzhen Chapter. He was selected as a Pengcheng Scholar Distinguished Professor, Shenzhen. He was a recipient of the Shenzhen Overseas High-Caliber Personnel Level B ("Peacock Plan Award" B) and Shenzhen High-Level Professional Talent (Local Leading Talent). He received the 2016 Shenzhen Science and Technology Progress Award and the 2017 Guangdong Provincial Science and Technology Progress Award. He is also serving as an Associate Editor for the IEEE NETWORK, the *International Journal of Communication Systems*, and *China Communications*.

Sai-Wai Wong (Senior Member, IEEE) received the B.S. degree in electronic engineering from The Hong Kong University of Science and Technology, Hong Kong, in 2003, and the M.Sc. and Ph.D. degrees in communication engineering from Nanyang Technological University, Singapore, in 2006 and 2009, respectively.

From July 2003 to July 2005, he was an Electronic Engineer to lead the Electronic Engineering Department in China with two Hong Kong manufacturing companies. From May 2009 to October 2010, he was a Research Fellow with the ASTAR Institute for Infocomm Research, Singapore. Since 2010, he was an Associate Professor and later become a Full Professor at the School of Electronic and Information Engineering, South China University of Technology, Guangzhou, China. From July 2016 to September 2016, he was a Visiting Professor with the City University of Hong Kong, Hong Kong. Since 2017, he has been a Full Professor with the College of Electronics and Information Engineering, Shenzhen University, Shenzhen, China. He has authored or coauthored more than 200 articles in international journals and conference proceedings. His current research interests include RF/microwave circuit and antenna design.

Dr. Wong was a recipient of the New Century Excellent Talents in University awarded by the Ministry of Education of China in 2013 and the Shenzhen Overseas High-Caliber Personnel Level C in 2018.

Chunxu Mao (Member, IEEE) received B.S. degree in communication engineering from the Guilin University of Electronic and Technology, Guilin, China, in 2010, the M.E. degree in RF and microwave engineering from the South China University of Technology, Guangzhou, China, in 2013, and the Ph.D. degree in electronic engineering from the University of Kent, Canterbury, U.K., in 2018.

From January 2018 to August 2019, he was a Research Fellow with the Computational Electromagnetics and Antennas Research Laboratory (CEARL), Pennsylvania State University, State College, PA, USA. In September 2019, he joined the Institute for Communication Systems (ICS), Home of the 5G Innovation Center (5GIC), University of Surrey, Guildford, U.K., as a Senior Research Fellow. His research interests include filtering antenna integration, metamaterial antennas, satellite antenna array, millimeter-wave antennas, and wearable antennas.

Dr. Mao served as the Session Chair for APS 2019, Atlanta. He was a recipient of the Outstanding Master Thesis Award of Guangdong Province, China, in 2014. He serves as a peer-reviewer in tens of journals, including the IEEE TRANSACTIONS ON ANTENNAS AND PROPAGATION, the IEEE TRANSACTIONS ON MICROWAVE THEORY AND TECHNIQUES, and the IEEE ANTENNAS WIRELESS PROPAGATION LETTERS.

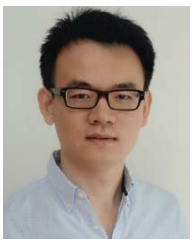

Lei Ge (Senior Member, IEEE) was born in Jiangsu, China. He received the B.S. degree in electronic engineering from the Nanjing University of Science and Technology, Nanjing, China, in 2009, and the Ph.D. degree in electronic engineering from the City University of Hong Kong, Hong Kong, in 2015.

From September 2010 to July 2011, he was a Research Assistant with the City University of Hong Kong. From April 2015 to October 2015, he was a Post-Doctoral Research Fellow with the State Key Laboratory of Millimeter Waves, City University of Hong Kong. He is currently an Assistant Professor with Shenzhen University, Shenzhen, China. His current research interests include patch antennas, base station antennas, reconfigurable antennas, MIMO antennas, millimeter-wave antennas, and multiband antennas.

Dr. Ge received the Honorable Mention at the Student Contest of 2012 IEEE APS-URSI Conference and Exhibition held in Chicago, USA, and the First Prize in the Student Innovation Competition of the 2014 IEEE International Workshop on Electromagnetics (IEEE iWEM) held in Sapporo, Japan, in 2014. He was a recipient of the IEEE Antennas and Propagation Society Outstanding Reviewer Award from 2017 to 2018. He was a TPC member and the session chair for several international conferences.

Steven (Shichang) Gao (Fellow, IEEE) received the Ph.D. degree from Shanghai University, Shanghai, China, in 1999.

He is currently a Full Professor and the Chair in RF and microwave engineering and the Director of Graduate Studies at the School of Engineering and Digital Arts, University of Kent, Canterbury, U.K. His research interests include smart antennas, phased arrays, MIMO, reconfigurable antennas, broadband/multiband antennas, satellite antennas, RF/microwave/millimeter-wave/terahertz circuits, mobile communications, satellite communications, UWB radars, synthetic aperture radars, the Internet of Things, and sensors for healthcare. He coauthored or coedited three books, *Space Antenna Handbook* (Wiley, 2012), *Circularly Polarized Antennas* (IEEE-Wiley, 2014), *Low-Cost Smart Antennas* (Wiley, 2019), and over 400 articles. He holds ten patents.

Dr. Gao is a fellow of the Royal Aeronautical Society, U.K., and the Institution of Engineering and Technology, U.K. He was the General Chair of LAPC 2013 and an Invited Speaker at many conferences. He serves as an Associate Editor for several international journals, such as the IEEE TRANSACTIONS ON ANTENNAS AND PROPAGATION, *Radio Science*, *Electronics Letters*, and *IET Circuits, Devices and Systems*, and the Editor-in-Chief for John Wiley & Sons Book Series on Microwave and Wireless Technologies. He was a Distinguished Lecturer of the IEEE Antennas and Propagation Society.